D-Atom Products in Predissociation of CD_2CD_2OH from the 202−215 nm Photodissociation of 2-Bromoethanol

L.W. Edwards, M. Ryazanov, and H. Reisler*

Department of Chemistry, University of Southern California, Los Angeles, California 90089-0482, USA

S. J. Klippenstein

Chemical Sciences and Engineering Division, Argonne National Laboratory, Argonne, Illinois 60439, USA

Received: January 8, 2010; Revised Manuscript Received: March 12, 2010

Experimental observations of D fragments from the predissociation of rovibrationally excited partially deuterated 2-hydroxyethyl radicals, CD_2CD_2OH, are reported, and possible dissociation channels are analyzed by theory. The radicals are produced by photolysis of 2-bromoethanol at 202−215 nm, and some of them have sufficient internal energy to predissociate. D fragments are detected by 1 + 1′ REMPI and their TOF distributions are determined. They can be associated with vinyl alcohol and/or acetaldehyde cofragments. From analysis of the maximum velocities and kinetic energies of the observed D fragments it is concluded that they originate from the decomposition of CD_2CD_2OH, but the experimental resolution is insufficient to distinguish between the two possible channels leading to D products. Theoretical analysis and RRKM calculations of microcanonical dissociation rates and branching ratios for the range of available excess energies (up to 5000−8000 cm^{-1} above the OH + C_2D_4 threshold) indicate that the D-producing channels are minor (about 1%) compared to the predominant OH + C_2D_4 channel, and the branching ratio for D production is more favorable when the reactant radicals have low rotational energy. The vinyl alcohol channel is strongly favored over the acetaldehyde channel at all excess energies, except near the threshold of these channels.

1. Introduction

The chemistry of hydroxyethyl radicals and their dissociation products is important in combustion and atmospheric chemistry.[1–20] Acetaldehyde and vinyl alcohol products have been identified in the decomposition of the 1- and 2-hydroxyethyl structural isomers (CH_3CHOH and CH_2CH_2OH, respectively), in addition to the major decomposition channel of CH_2CH_2OH to CH_2CH_2 + OH.[3,4,12,13,15,20] Of particular interest is the vinyl alcohol product, CH_2CHOH. Vinyl alcohol tautomerizes readily to the more thermodynamically stable acetaldehyde isomer upon storage and was previously postulated to exist only as a transient intermediate in chemical reactions. Despite high barriers to isomerization in the gas phase, it has been excluded from standard models of hydrocarbon oxidation.[12] Its recent discovery in significant concentrations in flames, however, as well as its identification as a dissociation product in electronically excited 1-hydroxyethyl radicals, has underscored the importance of this molecule in combustion.[3,4,12,13,15,20] The presence of the acetaldehyde tautomer in combustion reactions is well established.

The addition of OH to C_2H_4,[3,12,15,19,20] which can lead to formation of vinyl alcohol in flames, has been the subject of both experimental and theoretical studies. The reverse reaction is dominant in the dissociation of CH_2CH_2OH, as has been demonstrated before by using photolysis of haloethanols to generate 2-hydroxyethyl radicals.[6,8] Theoretical predictions assert, however, that other dissociation pathways of CH_2CH_2OH, such as dissociation to vinyl alcohol and acetaldehyde, can also play a role.[4,16,20] To date, no report has been published on dissociation pathways leading to H fragments. The three relevant channels are:

$$CH_2CH_2OH \rightarrow CH_2CH_2 + OH \text{ (major channel)} \quad (1)$$

$$D_{M-OH} = 1.14 \text{ eV } (109.6 \text{ kJ/mol})$$

$$CH_2CH_2OH \rightarrow CH_2CHOH + H \text{ (vinyl alcohol channel)} \quad (2)$$

$$D_{M-H} = 1.18 \text{ eV } (113.8 \text{ kJ/mol})$$

$$CH_2CH_2OH \rightarrow CH_3CHO + H \text{ (acetaldehyde channel)} \quad (3)$$

$$D_{M-H} = 0.76 \text{ eV } (72.8 \text{ kJ/mol})$$

where D_{X-Y} is the dissociation energy of channel XY → X + Y. Relevant energies and barriers based on the calculations of Senosiain et al.[4] are summarized in Figure 1. Channel 1 dominates at energies close to the dissociation threshold and has been observed in secondary dissociation of rovibrationally excited CH_2CH_2OH generated by UV photolysis of haloalcohols.[6,8] In these studies it is concluded that a large fraction of the CH_2CH_2OH radicals are generated in high rotational states, which are less easily coupled to the C−H bond cleavage coordinate. According to the rate calculations of Senosiain et al.,[4] other channels, in particular the vinyl alcohol channel, should become more important with increasing energy above the initial photolysis threshold. For example, in the 202 nm

* To whom correspondence should be addressed. E-mail: reisler@usc.edu. Phone: 213-740-7071. Fax: 213-740-3972.

10.1021/jp100203v
Published on Web 04/09/2010

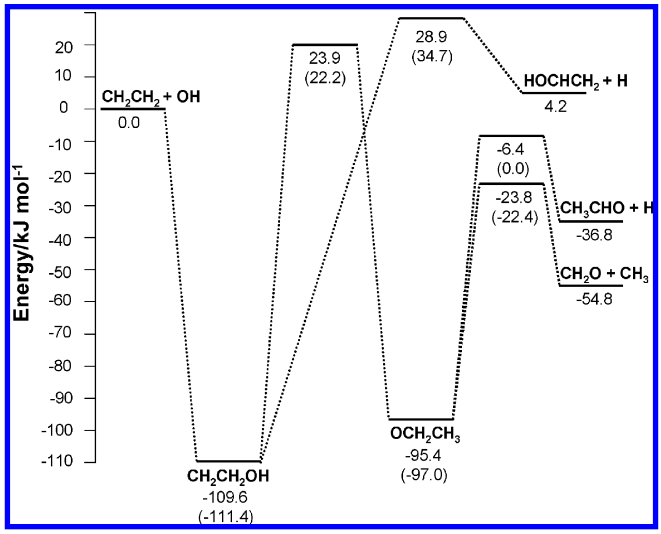

Figure 1. Schematic energy diagram for the decomposition of CH_2CH_2OH. Energies (in kJ/mol) are from ref 4. The corresponding barriers for CD_2CD_2OH, calculated in this work, are given in parentheses.

photolysis of $BrCH_2CH_2OH$ where there is ~3.14 eV available to products after C−Br photolysis (see below), vinyl alcohol can comprise a few percent of the products as discussed below.

CH_2CH_2OH radicals can be produced efficiently by photolysis of haloethanols.[5−8,21] Hintsa et al. photolyzed $BrCH_2CH_2OH$ at 193 nm and, using time-of-flight (TOF) spectroscopy, observed intact CH_2CH_2OH products with high kinetic and internal energies.[8] Moreover, they concluded that some of the radicals had high rotational excitation that was not available for predissociation on the experimental time scale. Predissociation of "hot" radicals (i.e., those produced with lower product kinetic energies/higher internal energies) to CH_2CH_2 + OH was detected by electron impact mass spectroscopy.[8] Sapers and Hess dissociated $BrCH_2CH_2OH$ and ICH_2CH_2OH and detected OH fragments by laser induced fluorescence (LIF).[6] They concluded that following photolysis of $BrCH_2CH_2OH$ at 202 nm, OH radicals were produced by predissociation of internally excited CH_2CH_2OH, whereas following ICH_2CH_2OH photolysis at 266 nm, absorption of a second 266 nm photon by CH_2CH_2OH was the main source of OH. Chandler et al. used photofragment imaging of ground-state $Br(^2P_{3/2})$ and spin−orbit excited $Br^*(^2P_{1/2})$ (hereafter denoted by Br and Br*, respectively) and determined the maximum and minimum kinetic energies of fragments produced in the 205 nm photolysis of bromoethanol.[5] Butler and co-workers carried out similar imaging experiments at 193 nm with higher resolution and concluded that Br was the main product.[21] A recent imaging study of ICH_2CH_2OH photolyzed at 253−298 nm[7] has shown that CH_2CH_2OH from the major dissociation channel to $I^*(^2P_{1/2})$ + CH_2CH_2OH does not undergo significant secondary dissociation. However, the authors conclude that 45−60% of the CH_2CH_2OH radicals correlated with $I(^2P_{3/2})$ do dissociate as a result of second photon absorption or dissociative photoionization. On the basis of the published room temperature absorption spectrum of CH_2CH_2OH between 210 and 265,[1] it was suggested that the radical could absorb an additional photon at the 266 nm photolysis wavelength and dissociate.

In the present study, we report the detection of D photofragments following 202−215 nm photolysis of $BrCD_2CD_2OH$ and conclude that they are generated by predissociation of internally excited CD_2CD_2OH. The partially deuterated product was used in order to distinguish between O- and C-bound hydrogens, and also to improve the signal-to-noise ratio in the experiment. D atoms were detected by 1 + 1′ resonance enhanced multiphoton ionization (REMPI) via its strong Lyman-α transition (~121.6 nm), and their TOF distributions were determined. Bromoethanol was chosen as the precursor because it absorbs strongly around 202 nm, and at this wavelength even after cleavage of the C−Br bond a fraction of the product 2-hydroxyethyl radicals should contain enough internal energy to predissociate via both the OH and D product channels.[4,20] D fragment maximum velocities and kinetic energies are used here to infer dissociation pathways. The theoretical calculations predict the energy dependence of the branching between channels 1−3 in CD_2CD_2OH dissociation via RRKM calculations based on the model of ref 4.

2. Experimental Details

The experimental apparatus has been described elsewhere and will be discussed only briefly here.[13,22] D fragments are generated following photolysis of $BrCD_2CD_2OH$ at wavelengths 202−215 nm. $BrCD_2CD_2OH$ (Aldrich, 98 atom % D, used without further purification) is evaporated to its vapor pressure of about 3 Torr at 25 °C into a 4 L glass bulb filled with He to a final pressure of 1 atm. A piezoelectrically driven pulsed nozzle operating at 10 Hz introduces this mixture to the source region of the differentially pumped vacuum chamber. The source chamber is pumped by a diffusion pump (Varian, VHS-6) equipped with a liquid nitrogen cooled trap, and the detection chamber by a turbomolecular pump (Leybold, Turbovac 361). The molecular beam is cooled in a supersonic expansion to an estimated rotational temperature of 10−15 K[22] and passes through a skimmer (Beam Dynamics, 1.51 mm diameter) into the detection chamber, where the $BrCD_2CD_2OH$ molecules are photolyzed and the D photofragments probed by counterpropagating laser beams aligned perpendicular to the molecular beam. Detection of D atoms eliminates many of the problems associated with H signals from photolysis of background hydrocarbons.

The pump (photolysis) radiation is generated by a Nd:YAG-pumped dye laser system (Continuum, PL8000/ND6000). Laser radiation at wavelengths 202−215 nm is generated by doubling the fundamental output of Rhodamine 640 or DCM dye in a KDP "C" (54.9°) crystal (Inrad), passing the output through a multiple-order wave plate, and then mixing the fundamental and doubled radiation in a BBO "0" (68.5°) crystal (Inrad). To meet the sum-frequency generation conditions, the doubled light and the fundamental light must have vertical polarization. However, the doubled light generated in the KDP crystal is polarized horizontally. Placing the wave plate on a rotatable mount allows for selection of the specific angles at which the doubled light becomes nearly vertically polarized, and the fundamental retains a large component of its initial polarization.

The photolysis laser radiation is focused into the detection chamber using a 25 cm focal length (f.l.) lens. The final laser output is polarized perpendicular to the TOF detector axis. Previous work indicated that photolysis of bromoethanol leads to a nearly isotropic distribution of Br fragments,[5,8,21] and the angular distributions of the D atoms, which are generated by slow secondary predissociation, are unlikely to depend on pump laser polarization.

The D fragments are detected by 1 + 1′ REMPI via the Lyman-α transition. The output of a Nd:YAG pumped dye laser system (Continuum, NY81/ND6000) pumping LDS 751 dye is doubled in a KDP "D" (46.6°) crystal (Inrad) to produce 6 mJ of

365 nm light that is then focused (20 cm f.l. lens) into a Kr/Ar tripling cell in which phase matching conditions are met by slow addition of argon to 200 Torr of krypton, until the scattered tripled light and the deuterium signal are observed at total pressures of 900−1000 Torr. The tripled 121.6 nm radiation, along with the residual 365 nm light, is focused in the detection chamber using a MgF_2 7.5 cm f.l. lens.

The D^+ ions are accelerated toward the detector perpendicularly to the laser and molecular beams by a static electric field, as described before,[13] and reach a multichannel plate detector (MCP, Galileo, 25 mm diameter) installed at the end of the 18 cm TOF tube. The TOF apparatus was calibrated by photolyzing HBr at 202, 205, 210, and 215 nm and monitoring the TOF distribution of H photofragments using the aforementioned 1 + 1′ REMPI detection scheme. The experimental calibration constant for H was scaled according to mass ratio to obtain the calibration constant 340 (m/s)/ns for D. The experimental broadening of the TOF spectra was 1.5−3 ns (mainly due to detection laser pulse width), corresponding to 750 ± 250 m/s in D velocity scale. This experimental arrangement does not give good velocity resolution for D ions with velocities below ~8000 m/s.[13] However, because the D fragments arise from secondary fragmentation, they have a wide range of energy distributions, and little information is gained from increasing the resolution for slow D fragments. On the other hand, the fastest fragments (i.e., the ones with the highest kinetic energy and correspondingly low internal energy in the molecular cofragment) correspond to higher kinetic energy release in the C-D bond cleavage for those CD_2CD_2OH radicals with the highest internal energy. The maximum observed kinetic energy at each photolysis wavelength can, thus, help identify the dissociation channel(s) leading to D atoms. Some uncertainty is implicit in the interpretation of the kinetic energy spectra owing to the detection of a secondary process that proceeds only after the primary C−Br photolysis step. Therefore, calculations were included in the analysis in order to support the experimental findings.

Due to the nature of the dissociation pathways, both of which occur via D loss from the α-carbon, isotopic substitution cannot provide any further insight as to the identities of the fragments. Nor can the cofragments be identified using their ionization potentials, since under our experimental conditions they cannot be ionized with enough efficiency to detect. To the best of our knowledge, however, this is the first report of D products from CD_2CD_2OH via C−D bond cleavage.

It is important to establish that the D fragments are generated following one-photon absorption in bromoethanol, since this information, along with thermochemical considerations, is used to determine the maximum velocity of the detected D^+ ions. It is therefore mandatory to suppress as much as possible multiphoton processes by reducing the pump pulse energy. This was achieved by moving the photolysis focal point away from the D detection region. Under these conditions the D^+ signal intensities increased linearly with increasing pump pulse energy. The optimal focusing condition was determined by monitoring several ion peaks in the TOF spectra and moving the position of the photolysis lens until the ion peaks were still visible, but with intensities well below the maximum. When monitoring the D^+ velocity distribution at the focal region of the photolysis lens, a tail at high velocities, presumably from generation of D products by multiphoton processes, begins to grow in at photolysis laser pulse energies exceeding 100 μJ. Under our defocused conditions, the high-velocity tail is almost absent when laser pulse energies are kept at <50 μJ before the 25 cm lens. In the reported experiments, the pump laser pulse energies are always limited to 20−25 μJ, which is the lowest laser power at which an adequate signal-to-noise ratio can still be obtained. Thus, fairly loose focusing conditions were used in combination with low laser power to optimize conditions for one-photon photolysis of $BrCD_2CD_2OH$.

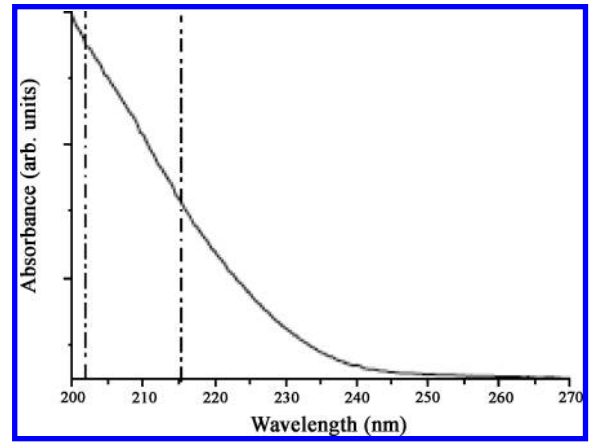

Figure 2. Absorption spectrum of gas phase 2-bromoethanol. The dashed lines indicate the 202−215 nm wavelength range of the present experiments.

Other sources of deuterium production were also considered and ruled out. No detectable background signal was observable from the photoysis laser alone, and the small deuterium background from the probe laser was subtracted from the spectra, eliminating the possibility of contributions from absorption of the Lyman-α radiation by $BrCD_2CD_2OH$ leading to primary D loss. D fragments from dissociation via the probe would exhibit much higher kinetic energies than those observed here. Direct D dissociation in the photolysis step was also considered. Absorption in the wavelength range 202−215 nm is to an antibonding orbital on the C−Br bond, which is also the weakest in the molecule, and the principal photolysis process is expected to involve cleavage of this bond.[23−26] Finally, variation of the delay time between the pump and probe lasers demonstrated that the probe ionized the D fragments created *after* the pump pulse and did not by itself produce any additional deuterium.

3. Results and Discussion

3.1. Absorption Spectrum of $BrCD_2CD_2OH$. The room temperature gas phase absorption spectrum of $BrCD_2CD_2OH$, shown in Figure 2, is broad and structureless. The absorption starts around 250 nm and increases monotonically to 200 nm. In halogen-containing hydrocarbons, the most weakly bound electrons are located in nonbonding orbitals on the halogen atoms, and the lowest-energy electronic excitation is to an antibonding σ* orbital on the carbon−halogen bond.[23−26] In the halogens and hydrogen halides, the first accessible σ* electronic excitation has been termed the "Q-complex" by Mulliken, and is comprised of three components labeled $^3Q_1$, $^3Q_0$, and $^1Q_1$.[24,27] For alkyl bromides, both singlet and triplet states are energetically accessible and absorption to both is allowed due to spin−orbit coupling.[25] In the dissociation both the ground state Br and electronically excited Br* can be generated.[5,8,21,25] Br* is correlated with the $^3Q_0$ state, which is accessible via a parallel transition, whereas Br is correlated with the $^1Q_1$ and $^3Q_1$ states, excited via a perpendicular transition.[25] In the alkyl iodides, due

to the strong spin−orbit coupling in iodine, the $^3Q_0$ state carries most of the oscillator strength at the center of the absorption band, and indeed, a study on ICH_2CH_2OH photolysis at 266 nm gave 75% I* product.[7] However, in molecules for which spin−orbit coupling is weaker, the parallel transition becomes less allowed. Some Br* product was observed in $BrCH_2CH_2OH$ photolysis at 193 and 205 nm, but the major product was ground state Br.[5,21] It is possible, of course, that at different wavelengths the three excited states contribute in different proportions to the absorption. However, based on the 193 and 205 nm results, we assume that Br atoms in their $^2P_{3/2}$ ground state are the major dissociation products. It is interesting to note that almost no angular anisotropy has been observed in the Br product distribution.[5,8,21] It has been suggested that this may be due to a large geometry change upon dissociation and not to the nature of the electronic absorption or a long lifetime.[8]

3.2. Mass Spectrum. Before discussing detection of D-atom fragments, we describe briefly survey mass spectra obtained at photolysis wavelengths 202−215 nm. To be able to observe species other than D atoms, the ionization wavelength was shifted slightly off-resonance from the 121.6 nm D peak. The main ion peaks were at $m/z = 47$ and 49, corresponding to the masses of CD_2CDOH (or CD_2HCDO) and CD_2CD_2OH. Additionally, smaller peaks corresponding to the masses of $^{79}BrCD_2CD_2OH^+$ and $^{81}BrCD_2CD_2OH^+$ ($m/z = 128$ and 130) were observed. There can be more than one source of the $m/z = 47$ and 49 peaks, which may derive either from ionization of dissociation products of $BrCD_2CD_2OH$ or from dissociative ionization of $BrCD_2CD_2OH$ (i.e., fragmentation of $BrCD_2CD_2OH^+$ ions generated by multiphoton absorption).[28] Unfortunately, the signal levels for $CD_2CD_2OH^+$ or CD_2CDOH^+ were small, and D was the only fragment ion detected with signal-to-noise sufficient to obtain TOF distributions.

3.3. Analysis of D-fragment Velocity and Energy Distributions. The main dissociation sequence responsible for production of D fragments from secondary predissociation of "hot" CD_2CD_2OH radicals following $BrCD_2CD_2OH$ photolysis is:

$$BrCD_2CD_2OH \xrightarrow{h\nu} CD_2CD_2OH^* + Br \quad (4)$$

$$CD_2CD_2OH^* \rightarrow CD_2CDOH + D \quad (5)$$

$$\rightarrow CD_2HCDO + D \quad (6)$$

where $CD_2CD_2OH^*$ denotes radicals with sufficient internal energy to dissociate.

Our TOF results can be converted straightforwardly to laboratory frame velocity distributions of D fragments. The velocity distributions obtained from the TOF distributions at 202−215 nm photolysis are displayed in Figure 3. To identify the dissociation channel(s) responsible for D products, we use energy conservation:

$$KE_{D+M} = h\nu - (D_{Br-R} + KE_{Br+R} + E_{Br} + D_{D-M} + E_M) \quad (7)$$

Here CD_2CD_2OH is denoted by R, and M denotes either of the two molecular cofragments: CD_2CDOH or CD_2HCDO (reactions 5 and 6). KE_{X+Y} is the kinetic energy release in the XY → X + Y dissociation process, $h\nu$ is the photon energy, and E_X is the internal energy of cofragment X. Because we are interested only in the maximum velocity and correspondingly maximum kinetic energy, we set $E_M = 0$ and $E_{Br} = 0$ (see below).

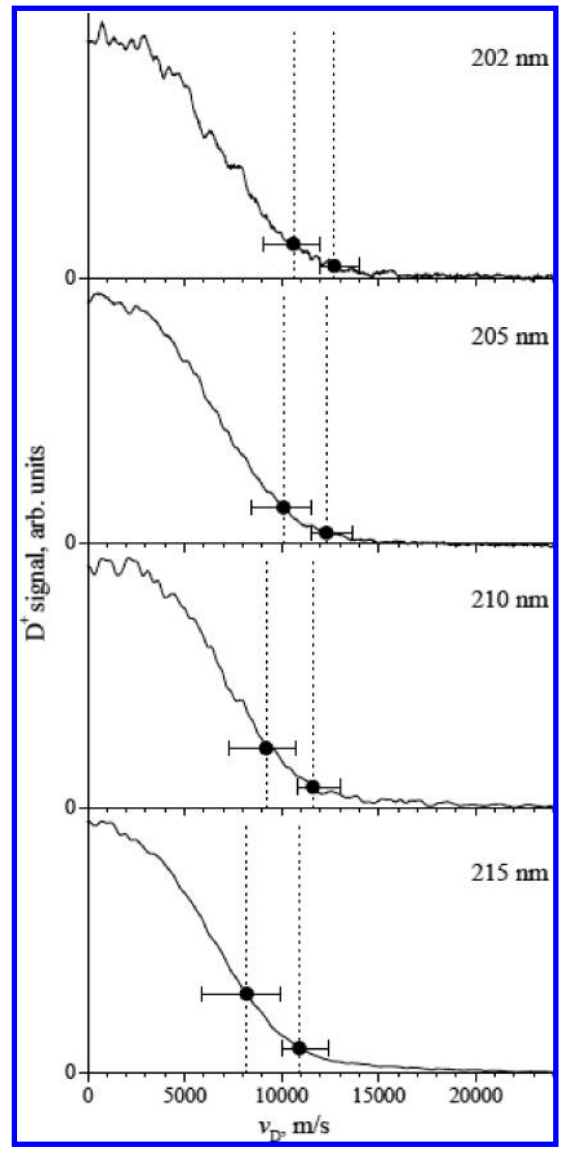

Figure 3. Experimental TOF distributions, converted to velocity scale, for D atoms from secondary dissociation of CD_2CD_2OH radicals produced by photolysis of $BrCD_2CD_2OH$ at 202, 205, 210, and 215 nm. Predicted maximum velocity limits for reactions 5 and 6 (lower and higher values, respectively) are indicated by vertical dotted lines and solid circles with error bars.

For the sequence of steps 4 and 5 + 6, the final D-atom velocity v_D is determined by the velocities v_R of the radicals generated in reaction 4 (in the laboratory frame) and the velocities $v_D^{(R)}$ of D atoms from reactions 5 and/or 6 (in the radical frame of reference):

$$\vec{v}_D = \vec{v}_R + \vec{v}_D^{(R)} \quad (8)$$

Using momentum conservation, the velocities of the radical in the laboratory frame and of the D atom in the radical frame, obtained from the corresponding kinetic energy release of each process, are given by:

$$v_R = \sqrt{\frac{2KE_{\mathrm{Br+R}}}{m_{\mathrm{R}}\left(1+\frac{m_{\mathrm{R}}}{m_{\mathrm{Br}}}\right)}}, \quad v_{\mathrm{D}}^{(\mathrm{R})} = \sqrt{\frac{2KE_{\mathrm{D+M}}}{m_{\mathrm{D}}\left(1+\frac{m_{\mathrm{D}}}{m_{\mathrm{M}}}\right)}} \tag{9}$$

where m_X denotes the mass of each fragment. The kinetic energy release depends on the partitioning of the initial photon energy $h\nu$ among the available degrees of freedom in reaction 4:

$$h\nu = D_{\mathrm{Br-R}} + KE_{\mathrm{Br+R}} + E_{\mathrm{R}} \tag{10}$$

$$E_{\mathrm{R}} = D_{\mathrm{D-M}} + KE_{\mathrm{D+M}} \tag{11}$$

Recognizing that CD_2CD_2OH is created with a broad range of internal energies, the velocity distribution of product D atoms is not unique but derives from a superposition of these distributions for the various internal energies of the radicals. Therefore, it is impossible to reconstruct an exact velocity distribution in reactions 5 and/or 6 from the TOF measurements.

However, we can easily estimate the *maximum* velocity of the D atoms for each dissociation channel. From eqs 8−11 this velocity is:

$$v_{\mathrm{D}} = \sqrt{\frac{2KE_{\mathrm{Br+R}}}{m_{\mathrm{R}}\left(1+\frac{m_{\mathrm{R}}}{m_{\mathrm{Br}}}\right)}} + \sqrt{\frac{2[h\nu - (D_{\mathrm{Br-R}} + D_{\mathrm{D-M}}) - KE_{\mathrm{Br+R}}]}{m_{\mathrm{D}}\left(1+\frac{m_{\mathrm{D}}}{m_{M}}\right)}} \tag{12}$$

This velocity depends on the kinetic energy release in the initial photolysis process (4). Figure 4 shows an example of such dependence for 205 nm photolysis, which is the only wavelength in this study for which the limits of $KE_{\mathrm{Br+R}}$ have been published.[5] The figure shows that lower *KE* in step 4 (i.e., higher E_R) correlates with higher D velocity (due to higher *KE* in eq 11).

However, data obtained from photolysis at 205 and 193 nm[5,8,21] indicate that the kinetic energy release for products of reaction 5 is generally high, peaking around 1.5 eV for either λ_{phot} wavelength. The lower limits of the observed *KE*′s for Br and Br* products are summarized in Table 1. The difference in the minimum observed values of *KE* for different wavelengths apparently does not exceed the experimental errors. Results on ICH_2CH_2OH photolysis also show that the lower limit of *KE* is nearly constant for a broad range of photolysis wavelengths (258−298 nm).[7] Thus a value of $KE_{\mathrm{Br+R}} = 0.95 \pm 0.10$ eV was used to establish limits on the maximum velocity of D fragments produced by reactions 5 and 6 for all wavelengths in the present study. This is indicated in Figure 4 with horizontal error bars for each reaction.

The energy considerations given by eqs 10 and 11 require knowledge of the dissociation energies for steps 4−6. However, the final equation, eq 12, contains only the *sum* of $D_{\mathrm{Br-R}}$ and $D_{\mathrm{D-M}}$, that is, the energy $\Delta_r E$ of the overall reaction

$$\mathrm{BrR} \rightarrow \mathrm{Br} + \mathrm{D} + \mathrm{M} \tag{13}$$

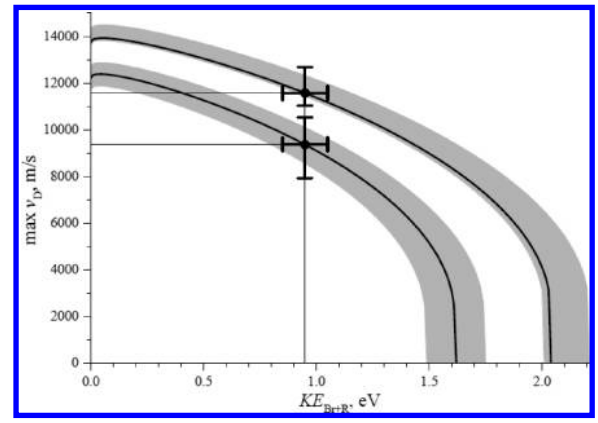

Figure 4. Maximum allowed laboratory frame velocity of D atoms as a function of kinetic energy release in the photolysis reaction 4 at 205 nm.. Lower and upper curves correspond to reactions 5 and 6, respectively. See the text for details.

TABLE 1: Values of Minimum Kinetic Energy Release in Photolysis Step

reference	λ_{phot} (nm)	min $KE_{\mathrm{Br+R}}$ (eV)	min $KE_{\mathrm{Br^*+R}}$ (eV)
5	205	1.08±0.06	1.17±0.06
8	193	0.85	
21	193	1.00	1.05

TABLE 2: Maximum Velocities Expected for Reactions 6 and 7

		max v_{D} (m/s)	
λ_{phot} (nm)	$h\nu$ (eV)	vinyl alcohol	acetaldehyde
202	6.138	9900^{+1100}_{-1300}	$12\,000^{+1100}_{-500}$
205	6.048	9400^{+1200}_{-1400}	$11\,600^{+1100}_{-500}$
210	5.904	8500^{+1300}_{-1700}	$10\,900^{+1200}_{-600}$
215	5.767	7500^{+1500}_{-2100}	$10\,200^{+1300}_{-600}$

which can be estimated from the enthalpies of formation of the atoms and the stable molecules: bromoethanol, vinyl alcohol, and acetaldehyde. The results, derived from a combination of experimental and theoretical data (see Appendix), are

$$\Delta_r E \equiv D_{\mathrm{Br-R}} + D_{\mathrm{D-M}} = 428 \pm 12\ \mathrm{kJ/mol} = 4.44 \pm 0.13\ \mathrm{eV}\ \text{(vinyl alcohol channel)}$$

$$= 387^{+3}_{-16}\ \mathrm{kJ/mol} = 4.01^{+0.03}_{-0.17}\ \mathrm{eV}\ \text{(acetaldehyde channel)}$$

These values are used in eq 12 to calculate the curves shown in Figure 4, where the shaded areas correspond to the associated uncertainties.

The total uncertainties in the determination of the maximum velocities of the D fragments, derived from the combination of uncertainties in the dissociation energies and in the lower limits of *KE* observed in the photolysis reaction 4, are indicated in Figure 4 by the vertical error bars. Table 2 summarizes the maximum D-fragment velocities expected for each dissociation channel at the investigated photolysis wavelengths. These values are also indicated in Figure 3.

Finally, we explain why we use only $E_{\mathrm{Br}} = 0$ in eq 4. Experimental results show that Br* products are also generated with high kinetic energies [Table 1],[5,21] and thus the maximum velocity of D atoms for reactions 4−6 associated with Br* is lower than for the corresponding Br channel.

3.4. Maximum Velocities of D Fragments and Dissociation Pathways. Figure 3, which displays the velocity distributions of D atoms obtained at 202, 205, 210, and 215 nm photolysis

wavelengths, also displays the maximum velocities for reactions 5 and 6, obtained as described in Section 3.3 and corrected for experimental broadening. In each plot the values at higher velocities correspond to reaction 6. The error bars include those in Table 2 as well as the experimental uncertainties. The high velocity limit of the distribution shifts slightly to lower velocities at longer photolysis wavelengths, as expected. No dramatic changes in the spectra are expected with wavelength variation because of the wide distribution of product kinetic and internal energies generated in the primary and secondary dissociation steps. Nevertheless, the agreement in all the plots between the maximum observed velocity values and those predicted by eq 12 reinforces our conclusion that the observed D fragments are products of reactions 5 and 6; that is, they derive from secondary dissociation of "hot" CD_2CD_2OH radicals. Further examination of the curves in Figure 3 identifies a small region at high velocities with a low fragment population whose maximum value corresponds to reaction 6, and a region displaying a large increase in fragment populations that begins at velocities estimated for the onset of reaction 5. It is thus reasonable that the favored process that produces D atoms is the vinyl alcohol channel (5) (see also below).

We notice, however, that in the velocity distributions obtained with 210 and 215 nm photolysis, a small tail persists that extends beyond the maximum velocity allowed for reaction 6. This tail, which does not seem to vary any more with reduction in laser power, may be the result of absorption of a second 210 or 215 nm photon by CD_2CD_2OH. Second photon absorption is likely to be more efficient at longer wavelengths because at low photolysis energies a larger fraction of long-lived CD_2CD_2OH radicals (i.e., those with energies either below the dissociation barrier or above it but with long dissociation lifetimes) are produced. As discussed previously,[6–8] a significant fraction of the radicals' internal energy is tied up in rotational motion, which does not couple well to the dissociation coordinates. These "rotationally metastable" radicals have a higher probability of absorbing a second photon and then dissociating to D products with very high velocities.[6,7] At shorter wavelengths, the "hotter" radicals dissociate faster and have a reduced probability for absorption of a second photon. Recent theoretical calculations of the electronic states of CH_2CH_2OH indicate that absorption to both Rydberg and valence states is possible at this wavelength range.[29] The existence of "rotationally metastable" radicals also reduces the branching ratio of the D-producing channels 5 and 6 relative to the lowest energy channel that gives OH + C_2H_4 (see below). Thus, the longer lifetime of the radical produced from 210 and 215 nm photolysis, in combination with the onset of an electronic absorption in CD_2CD_2OH, leads to the increased efficiency of two-photon processes at these wavelengths and the appearance of a high energy tail in the D fragment velocities that persists down to very low pump powers.

3.5. Theoretical Estimates of Product Branching Ratios. According to the calculations of Senosiain et al.[4] the dissociation energy of the CH_2CH_2OH radical to the lowest channel, reaction 1, is 1.14 eV, and the reaction proceeds without a reverse barrier. The theoretical work of Senosiain et al. couples high level electronic structure calculations and transition state theory with a master equation analysis for the kinetics of the CH_2CH_2 + OH reaction. The branching ratios arising from the collisionless limit of this analysis are at least qualitatively related to the present observation of the production of D atoms in the dissociation of CD_2CD_2OH. Figure 11 of ref 4 suggests that the vinyl alcohol + H channel dominates over the acetaldehyde + H channel and at high energies it also dominates over the formaldehyde + methyl channel.[4] That plot also appears to suggest the importance of a water + vinyl channel, but this channel arises largely from direct abstraction from ethylene by OH, which is not relevant to the present analysis. The consideration of ethylene + OH as the reactants in that work obscures the branching to that channel. However, examination of the underlying RRKM analysis suggests that the branching to that channel dominates the CH_2CH_2OH dissociation kinetics, with only a few percent branching to the H atom producing channels.

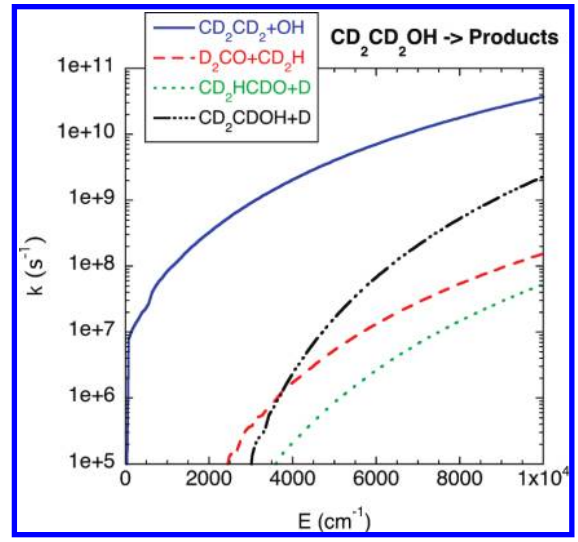

Figure 5. Dissociation rates of the CD_2CD_2OH radical to the different channels as indicated in the figure.

The underlying microcanonical RRKM analysis of ref 4 could be compared directly to the present observations. However, the partial deuteration may have some effect on the predicted rate constants and branching ratios. Thus, to properly compare with the present experiments, we have evaluated the rovibrational properties of the stationary points for the relevant partially deuterated species at the B3LYP/6-311++G(d,p) level, and the relevant reaction barriers for these species are included in parentheses in Figure 1. These rovibrational properties were then incorporated in a revised RRKM analysis for the partially deuterated species of interest here. Note that, in predicting the dissociation rates to D_2CO + CD_2H and to CD_2HCDO + D, we have simply multiplied the isomerization rate from CD_2CD_2OH to CD_2HCD_2O by the ratio of the decomposition rates to these channels (from CD_2HCD_2O) relative to the total decomposition rate from CD_2HCD_2O. This approach is accurate since the back isomerization from CD_2HCD_2O to CD_2CD_2OH is negligible.

As per the discussion in Section 3.4 and given the known reaction energies, the excess energies (relative to CD_2CD_2 + OH) in the 2-hydroxyethyl radical decomposition following photolysis at 202−215 nm will extend up to about 5000−8000 cm^{-1}. The present RRKM predicted microcanonical dissociation rates for the partially deuterated analogs of reactions 1−3 at these excess energies are shown in Figure 5 and these rates reflect mainly dissociation via reaction 1. These microcanonical rates are for radicals with a total angular momentum J of 4, and similar results are found for modestly larger total angular momentum. The reaction channels terminating in D products are minor, constituting no more than a few percent of all products. Nevertheless, we have no problem detecting these

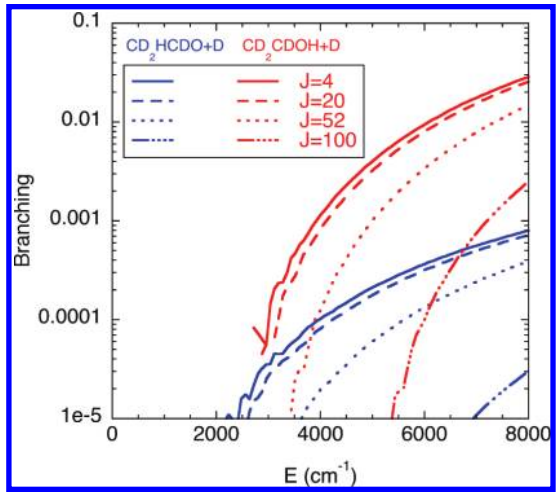

Figure 6. Branching ratios for the CD_2CDOH + D and CD_2HCDO + D channels for different rotational levels of the CD_2CD_2OH radical.

channels via the very sensitive 1 + 1′ REMPI scheme for H and D atoms.

The acetaldehyde product correlated with H(D) cofragments could not be discerned from vinyl alcohol in our study because dissociation to both species proceeds via C−D bond cleavage of the α-carbon and thus isotopic substitution would be of no help. Although the barrier to isomerization to the ethoxy radical that precedes dissociation to the acetaldehyde channel is slightly lower than that for direct dissociation to vinyl alcohol, the isomerization, which involves a tight transition state where the H atom is transferred from O directly to the β-carbon, is inefficient.[4,18,20] Additionally, the dissociation of CH_3CH_2O to the acetaldehyde product competes with the reaction that yields $H_2CO + CH_3$, which has a lower barrier (see Figure 1), and thus the latter should comprise the major dissociation channel of the ethoxy radical in both CH_2CH_2OH and CD_2CD_2OH.[4,20]

Our calculations show that vinyl alcohol should be the major dissociation product in channels leading to H (or D) fragments. The energy-dependent branching ratios for the two D-atom loss channels are illustrated in Figure 6 for radicals in rotational states J of 4, 20, 52, and 100. The branching to both these channels decreases with increasing J as the rotational barriers become more significant. Thus, the contributions of the D channels are largest for those "hot" 2-hydroxyethyl radicals that are born with modest rotational excitation. These are also the radicals that dissociate the fastest and whose products are likely to be observed in our detection region.

As shown in Figure 6, the branching to channel 6 (acetaldehyde) relative to channel 5 (vinyl alcohol) decreases with increasing energy. At an excess energy of 8000 cm^{-1}, which roughly corresponds to D fragments with maximum velocities, the branching to the acetaldehyde channel is predicted to be a few percent of that to the vinyl alcohol channel. This modest branching to reaction 6 is in reasonable agreement with the experimental TOF distributions in Figure 3, and with the conclusions of refs 4 and 20 of calculations for the fully hydrogenated radical. The increase in this relative branching with decreasing energy also matches well with the changes in the TOF distributions with increasing photolysis wavelength.

4. Summary

Experimental observations of D fragments from the predissociation of rovibrationally excited 2-hydroxyethyl radicals, CD_2CD_2OH, are reported and possible dissociation channels are analyzed by theory. The radicals are produced by photolysis of 2-bromoethanol at 202−215 nm. Previous results established that some of these radicals are generated with sufficient internal energy to undergo secondary dissociation, and the lowest dissociation channel to OH + ethylene was indeed observed previously.[6,8] Calculations have predicted that while the main dissociation channel is OH + ethylene, two minor channels may generate H or D atoms, one associated with vinyl alcohol and the other with acetaldehyde cofragments.[4,20]

In the present experiments, D fragments are detected by 1 + 1′ REMPI and their TOF distributions are determined. From analysis of the maximum velocities and kinetic energies of the observed D fragments it is concluded that they originate from the decomposition of CD_2CD_2OH, but the experimental resolution is insufficient to distinguish between the two possible channels leading to D products. Theoretical analysis and RRKM calculations of microcanonical dissociation rates and branching ratios for the range of available excess energies (up to 5000−8000 cm^{-1} above the OH + C_2D_4 threshold) indicate that: (i) the D-producing channels are minor compared to the OH + C_2D_4 channel, constituting at most a few percent; (ii) the branching ratio is more favorable toward these products when the reactant radicals have low rotational energy; and (iii) the vinyl alcohol channel is strongly favored over the acetaldehyde channel at all but the lowest excess energies.

Appendix

To apply eq 12, the values of the two dissociation energies D_{Br-R} and D_{D-M} are required. D_{Br-R} was estimated from C−Br bond energies in similar molecules to be 289 ± 8 kJ/mol.[28] In more recent work the standard enthalpy of dissociation was estimated at 305 ± 8 kJ/mol from a combination of experimental data and theoretical calculations.[30] No experimental data for the dissociation energy of the 2-hydroxyethyl radical are available. However, the sum of the dissociation energies that is required in eq 12 is equal to the energy of the net reaction 13, and the standard enthalpy of reaction 13 can be calculated straightforwardly.

The standard enthalpy of reaction needs to be corrected to obtain the energy of reaction at 0 K, and the isotopic differences in energies between the partially deuterated and the nondeuterated molecules should also be taken into account. The thermal corrections are composed of translational ($^3/_2RT$ for all species), rotational and vibrational ($^3/_2RT$ and H_v for molecules) contribu-

TABLE A1: Thermochemical Values Used in Evaluating Equation A1

species	$\Delta_f H^0$ (kJ/mol)	H_v(298.15 K) (kJ/mol (cm^{-1}))	ZPE (cm^{-1})	ZPE_D (cm^{-1})	$\Delta_D ZPE = ZPE_D - ZPE$ (kJ/mol (cm^{-1}))
$BrCH_2CH_2OH$	$-221.7^{+10}_{-0.7}$ [a]	5.89 (492)	15 353	12 451	−34.7 (2902)
Br	+111.81 ± 0.12 [b]				
H	+217.998 ± 0.006 [b]				
CH_2CHOH	-125.4^{+11}_{-2} [c]	2.15 (180)	12 211	10 178	−24.3 (2033)
CH_3CHO	$-166.2^{+0.7}_{-4.5}$ [d]	2.82 (236)	11 952	9950	−23.9 (2002)

[a] Reference 30. [b] Reference 37. [c] Reference 38. [d] Reference 39.

tions, and the $\Delta PV = \Delta nRT$ term. Isotopic corrections for the molecules are taken as differences in zero point vibrational energies (ZPE) of the corresponding isotopologs (Δ_DZPE). The expression used for the energy of reaction is:

$$\Delta_r E = \Delta_f H^0(\mathrm{Br}) + \Delta_f H^0(\mathrm{H}) + \Delta_f H^0(\mathrm{M}) - \Delta_f H^0(\mathrm{BrR}) - 5RT - H_v(\mathrm{M}) + H_v(\mathrm{BrR}) + \Delta_D\mathrm{ZPE}(\mathrm{M}) = \Delta_D\mathrm{ZPE}(\mathrm{BrR}) \quad \text{(A1)}$$

The vibrational enthalpies H_v and ZPE were calculated in the harmonic oscillator approximation from frequencies obtained by quantum chemical calculations at the B3LYP/aug-cc-pVTZ level using the Q-Chem software package.[31] The calculated frequencies were used because the experimental information is incomplete even for the nondeuterated species and is entirely missing for the deuterated analogs of interest. (However, for CD_2CDOH, 9 of 15 fundamental frequencies were measured in an argon matrix.)[32] The most complete set of spectroscopic constants (harmonic frequencies and anharmonic constants) derived from experimental data is available for CH_3CHO, and comparison of the experimental harmonic frequencies with the theoretical calculations shows an rms deviation of about 20 cm^{-1} and a best fit scaling factor of 0.999 ± 0.003. For $BrCH_2CH_2OH$ and CH_2CHOH, only the fundamental experimental frequencies are available.[33,34] The best fit of the theoretical harmonic frequencies to these data gives an rms deviation of 20 cm^{-1}, which is comparable to the discrepancies between different experimental determinations. The derived scaling factor (experimental fundamental/theoretical harmonic) is 0.964 ± 0.003, which is very close to the recommended scaling factor of 0.9676 for calculations of fundamental frequencies from B3LYP/aug-cc-pVTZ harmonic frequencies. This agreement suggests that the theoretical frequencies can be reliably used in calculations of the thermal and isotopic corrections. For this purpose the frequencies were scaled by 0.9867, the factor recommended for calculations of H_v and ZPE.[35]

The experimental values of the standard enthalpies of formation and the theoretically estimated H_v and ZPE are listed in Table A1. Note that the enthalpies of formation of the molecular species have asymmetric error bars. The reason for this is that the values listed in the table are the most recent results, believed to be the most reliable, and the smaller errors correspond to the reported error bars for those values. However, the discrepancies between the listed values and the earlier (but still apparently reliable) values[28,33,36] are larger than the estimated errors, so these differences are shown as larger error bars in one direction. Additionally, the enthalpy of formation of 2-bromoethanol refers to Gg, the most stable conformer. However, at room temperature in the gas phase a few percent of the molecules are in the Tt and Tg conformations, where G or T and g or t refer to gauche or trans configurations about the C−C and C−O bonds, respectively. These conformers have 4−6 kJ/mol higher energies.[34] Their contributions are also included in the error bars.

The error bars for the final results of the energy of the overall reaction 13 were obtained by assuming that the errors in the enthalpies of formation of the molecules are additive and all other errors are uncorrelated. The estimated errors in Table A1 (one standard deviation) are: 0.055 kJ/mol (5 cm^{-1}) for H_v(298.15 K) and 1.2 kJ/mol (100 cm^{-1}) for ZPEs according to ref 34.

Acknowledgment. The authors wish to thank Dr. Ksenia Bravaya for theoretical calculations of harmonic frequencies, Dr. Stephen Pratt and Dr. Boris Karpichev for helpful discussions, and Professor Laurie Butler for communicating results prior to publications. H.R. and S.J.K. acknowledge support of the Division of Chemical Sciences, Geosciences, and Biosciences, the Office of Basic Energy Sciences, the U.S. Department of Energy (grant DE-FG02-05ER15629 and contract No. DE-AC02-06CH11357, respectively).

References and Notes

(1) Anastasi, C.; Simpson, V.; Munk, J.; Pagsberg, P. *J. Phys. Chem.* **1990**, *94*, 6327.
(2) Liu, G. X.; Ding, Y. H.; Li, Z. S.; Fu, Q.; Huang, X. R.; Sun, C. C.; Tang, A. C. *Phys. Chem. Chem. Phys.* **2002**, *4*, 1021.
(3) Cool, T. A.; Nakajima, K.; Mostefaoui, T. A.; Qi, F.; McIlroy, A.; Westmoreland, P. R.; Law, M. E.; Poisson, L.; Peterka, D. S.; Ahmed, M. *J. Chem. Phys.* **2003**, *119*, 8356.
(4) Senosiain, J. P.; Klippenstein, S. J.; Miller, J. A. *J. Phys. Chem. A* **2006**, *110*, 6960.
(5) Chandler, D. W.; Thoman, J. W.; Hess, W. P. *Inst. Phys. Conf. Ser.* **1991**, 355.
(6) Sapers, S. P.; Hess, W. P. *J. Chem. Phys.* **1992**, *97*, 3126.
(7) Shubert, V. A.; Rednic, M.; Pratt, S. T. *J. Phys. Chem. A* **2009**, *113*, 9057.
(8) Hintsa, E. J.; Zhao, X. S.; Lee, Y. T. *J. Chem. Phys.* **1990**, *92*, 2280.
(9) Vakhtin, A. B.; Murphy, J. E.; Leone, S. R. *J. Phys. Chem. A* **2003**, *107*, 10055.
(10) Yamada, T.; Bozzelli, J. W.; Lay, T. *J. Phys. Chem. A* **1999**, *103*, 7646.
(11) Tully, F. P. *Chem. Phys. Lett.* **1988**, *143*, 510.
(12) Taatjes, C. A.; Hansen, N.; McIlroy, A.; Miller, J. A.; Senosiain, J. P.; Klippenstein, S. J.; Qi, F.; Sheng, L.; Zhang, Y.; Cool, T. A.; Wang, J.; Westmoreland, P. R.; Law, M. E.; Kasper, T.; Kohse-Hoinghaus, K. *Science* **2005**, *308*, 1887.
(13) Karpichev, B.; Edwards, L. W.; Wei, J.; Reisler, H. *J. Phys. Chem. A* **2008**, *112*, 412.
(14) Diau, E. W. G.; Lee, Y. P. *J. Chem. Phys.* **1992**, *96*, 377.
(15) Taatjes, C. A.; Hansen, N.; Miller, J. A.; Cool, T. A.; Wang, J.; Westmoreland, P. R.; Law, M. E.; Kasper, T.; Kohse-Hoinghaus, K. *J. Phys. Chem. A* **2006**, *110*, 3254.
(16) Sosa, C.; Schlegel, H. B. *J. Am. Chem. Soc.* **1987**, *109*, 4193.
(17) Hippler, H.; Viskolcz, B. *Phys. Chem. Chem. Phys.* **2000**, *2*, 3591.
(18) Zhu, R. S.; Park, J.; Lin, M. C. *Chem. Phys. Lett.* **2005**, *408*, 25.
(19) Tully, F. P. *Chem. Phys. Lett.* **1983**, *96*, 148.
(20) Xu, Z. F.; Xu, K.; Lin, M. C. *ChemPhysChem* **2009**, *10*, 972.
(21) Ratliff, B. J.; Womack, C. C.; Tang, X. N.; Landau, W. M.; Butler, L. J.; Szpunar, D. E.; *J. Phys. Chem. A* **2010**, DOI: 10.1021/jp911739a; ASAP.
(22) Aristov, V.; Conroy, D.; Reisler, H. *Chem. Phys. Lett.* **2000**, *318*, 393.
(23) Krajnovich, D.; Butler, L. J.; Lee, Y. T. *J. Chem. Phys.* **1984**, *81*, 3031.
(24) Mulliken, R. S. *Phys. Rev.* **1936**, *50*, 1017.
(25) Pence, W. H.; Baughcum, S. L.; Leone, S. R. *J. Phys. Chem.* **1981**, *85*, 3844.
(26) Mullikan, R. S. *Phys. Rev.* **1934**, *46*, 549.
(27) Mullikan, R. S. *Phys. Rev.* **1940**, *57*, 500.
(28) Ruscic, B.; Berkowitz, J. *J. Chem. Phys.* **1994**, *101*, 10936.
(29) Karpichev, B.; Koziol, L.; Diri, K.; Reisler, H.; Krylov, A. I. *J. Chem. Phys.* **2010**, *132*, 114308.
(30) Bernardes, C. E. S.; da Piedade, M. E. M.; Amaral, L. M. P. F.; Ferreira, A. I. M. C. L.; da Silva, M. A. V. R.; Diogo, H. P.; Cabral, B. J. C. *J. Phys. Chem. A* **2007**, *111*, 1713.
(31) Shao, Y.; Molnar, L. F.; Jung, Y.; Kussmann, J.; Ochsenfeld, C.; Brown, S. T.; Gilbert, A. T. B.; Slipchenko, L. V.; Levchenko, S. V.; O'Neill, D. P.; DiStasio, R. A.; Lochan, R. C.; Wang, T.; Beran, G. J. O.; Besley, N. A.; Herbert, J. M.; Lin, C. Y.; Van Voorhis, T.; Chien, S. H.; Sodt, A.; Steele, R. P.; Rassolov, V. A.; Maslen, P. E.; Korambath, P. P.; Adamson, R. D.; Austin, B.; Baker, J.; Byrd, E. F. C.; Dachsel, H.; Doerksen, R. J.; Dreuw, A.; Dunietz, B. D.; Dutoi, A. D.; Furlani, T. R.; Gwaltney, S. R.; Heyden, A.; Hirata, S.; Hsu, C. P.; Kedziora, G.; Khalliulin, R. Z.; Klunzinger, P.; Lee, A. M.; Lee, M. S.; Liang, W.; Lotan, I.; Nair, N.; Peters, B.; Proynov, E. I.; Pieniazek, P. A.; Rhee, Y. M.; Ritchie, J.; Rosta, E.; Sherrill, C. D.; Simmonett, A. C.; Subotnik, J. E.; Woodcock, H. L.; Zhang, W.; Bell, A. T.; Chakraborty, A. K.; Chipman, D. M.; Keil, F. J.; Warshel, A.; Hehre, W. J.; Schaefer, H. F.; Kong, J.; Krylov, A. I.; Gill, P. M. W.; Head-Gordon, M. *Phys. Chem. Chem. Phys.* **2006**, *8*, 3172.

(32) Rodler, M.; Blom, C. E.; Bauder, A. *J. Am. Chem. Soc.* **1984**, *106*, 4029.
(33) Joo, D. L.; Merer, A. J.; Clouthier, D. J. *J. Mol. Spectrosc.* **1999**, *197*, 68.
(34) Durig, J. R.; Shen, S.; Guirgis, G. A. *J. Mol. Struct.* **2001**, *560*, 295.
(35) Sinha, P.; Boesch, S. E.; Gu, C. M.; Wheeler, R. A.; Wilson, A. K. *J. Phys. Chem. A* **2004**, *108*, 9213.
(36) Traeger, J. C.; Djordjevic, M. *Eur. J. Mass Spec* **1999**, *5*, 319.
(37) Cox, J. D.; Wagman, D. D.; Medvedev, V. A. *CODATA Key Values for Thermodynamics*; Hemisphere Publishing Corp.: New York, 1989.
(38) da Silva, G.; Bozzelli, J. W. *J. Phys. Chem. A* **2006**, *110*, 13058.
(39) da Silva, G.; Kim, C. H.; Bozzelli, J. W. *J. Phys. Chem. A* **2006**, *110*, 7925.

JP100203V